Asociación Argentina
de Mecánica Computacional

Mecánica Computacional Vol XXV, pp. 2431-2449
Alberto Cardona, Norberto Nigro, Victorio Sonzogni, Mario Storti. (Eds.)
Santa Fe, Argentina, Noviembre 2006

STABILITY AND NUMERICAL RESULTS FOR A THERMOELASTIC JOINT-LEG-BEAM SYSTEM †

E. M. Cliff*, Z. Liu and R. D. Spies‡**

* Interdisciplinary Center for Applied Mathematics
Virginia Tech, Blacksburg, VA 24061-0531, USA

** Department of Mathematics and Statistics
University of Minnesota at Duluth, Duluth, MN 55812-3000, USA

‡ Instituto de Matemática Aplicada del Litoral, IMAL
CONICET -UNL , Güemes 3450, S3000GLN Santa Fe, Argentina
E-mail: rspies@imalpde.ceride.gov.ar

Key Words: Thermoelastic system, Truss structures, Rigidizable/Inflatable materials, Partial Differential Equations, Mechanics of Deformable Solids.

Abstract. *Rigidizable/Inflatable (RI) materials offer the possibility of deployable large space structures[5] and so are of interest in applications where large optical or RF apertures are needed. In particular, in recent years there has been renewed interest in inflatable-rigidizable truss-structures (see Figure 1) because of the efficiency they offer in packaging during boost-to-orbit. However, much research is still needed to better understand dynamic response characteristics, including inherent damping, of truss structures fabricated with these advanced material systems.*

One of the most important characteristics of such space systems is their response to changing thermal loads, as they move in/out of the Earth's shadow. We study the thermoelastic behaviour of a basic truss component consisting of two RI beams connected through a joint subject to solar heating.

† This research was supported in part by Defense Advanced Research Projects Agency/Special Projects Office (DARPA/SPO), NASA Langley Research Center and the National Institute for Aerospace of USA, under Grant NIA 2535, by the Consejo Nacional de Investigaciones Científica y Técnicas of Argentina, CONICET and by Universidad Nacional del Litoral, UNL, Santa Fe, Argentina.

1 THERMOELASTIC MODEL

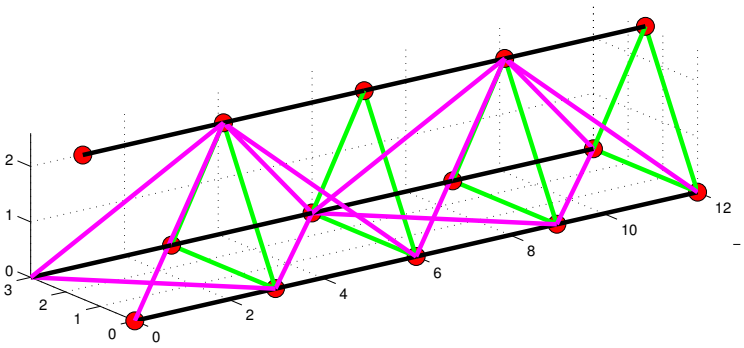

Figure 1: Truss-structure

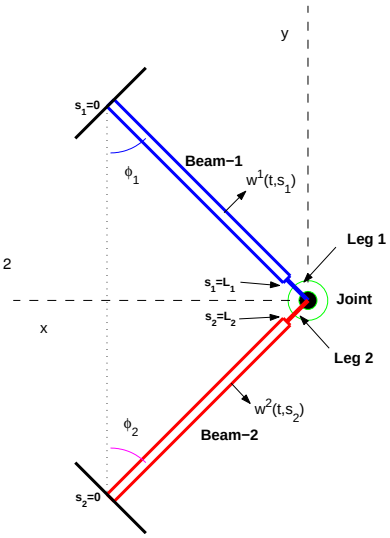

Figure 2: Basic truss component

The equations of motion for the Joint-Leg-Beam system depicted in Figure 2 has been derived in[1] as the following:

$$\rho_i A_i \frac{\partial^2 u^i(t,s_i)}{\partial t^2} = E_i A_i \frac{\partial^2 u^i(t,s_i)}{\partial s_i^2}, \qquad \rho_i A_i \frac{\partial^2 w^i(t,s_i)}{\partial t^2} = -E_i I_i \frac{\partial^4 w^i(t,s_i)}{\partial s_i^4} \tag{1}$$

$$\mathbf{M}\frac{d^2}{dt}\begin{bmatrix} x(t) \\ y(t) \\ \theta_1(t) \\ \theta_2(t) \end{bmatrix} = \mathbf{C}\begin{bmatrix} M_1(t) \\ N_1(t) \\ M_2(t) \\ N_2(t) \\ F_1(t) \\ F_2(t) \end{bmatrix} \text{ for time } t > 0 \text{ and spatial variable } s_i \in [0, L_i], \text{ where}$$

$$\mathbf{M} = \begin{pmatrix} m & 0 & -m_1 d_1 \cos\varphi_1 & m_2 d_2 \cos\varphi_2 \\ 0 & m & +m_1 d_1 \sin\varphi_1 & m_2 d_2 \sin\varphi_2 \\ -m_1 d_1 \cos\varphi_1 & m_1 d_1 \sin\varphi_1 & I_{1\ell}+m_1 d_1^2 & 0 \\ m_2 d_2 \cos\varphi_2 & m_2 d_2 \sin\varphi_2 & 0 & I_{2\ell}+m_2 d_2^2 \end{pmatrix}, \quad C = \begin{pmatrix} 0 & -\cos\varphi_1 & 0 & \cos\varphi_2 & \sin\varphi_1 & \sin\varphi_2 \\ 0 & \sin\varphi_1 & 0 & \sin\varphi_2 & \cos\varphi_1 & -\cos\varphi_2 \\ 1 & \ell_1 & 0 & 0 & 0 & 0 \\ 0 & 0 & 1 & \ell_2 & 0 & 0 \end{pmatrix}, \tag{2}$$

and the other functions and parameters are as follows: u^i, w^i: longitudinal and transversal displacement of the beam i; x, y: horizontal and vertical displacement of the joint's tip; θ_i: rotation angle of the leg i; $\rho_i, A_i, L_i, E_i, I_i$: mass density, cross section area, length, Young's modulus, moment of inertia of the beam i; μ_i, γ_i: damping coefficients; $m_i, d_i, \ell_i, I_{i\ell}$: mass, center of mass, length, moment of inertia of leg i; m_p: mass of the joint, $m = m_1 + m_2 + m_p$; φ_1: initial angle of leg 1 with positive y axis; φ_2: initial angle of leg 2 with negative y axis; $F_i(t)$: extensional force of beam i at the end $s_i = L_i$; $N_i(t)$: shear force of beam i at the end $s_i = L_i$; $M_i(t)$: bending moment of beam i at the end $s_i = L_i$. The beams are clamped at the

end $s_i = 0$. Thus the boundary conditions at $s_i = 0$ are

$$u^i(t,0) = w^i(t,0) = \frac{\partial w^i}{\partial s_i}(t,0) = 0, \qquad i = 1,2. \tag{3}$$

At the other end of the beam, we have geometric compatibility conditions that can be written in the form:

$$\begin{bmatrix} -\frac{\partial}{\partial s_1} w^1(t,L_1) \\ w^1(t,L_1) \\ -\frac{\partial}{\partial s_2} w^2(t,L_2) \\ w^2(t,L_2) \\ -u^1(t,L_1) \\ -u^2(t,L_2) \end{bmatrix} = \begin{bmatrix} \theta_1(t) \\ -x(t)\cos\varphi_1 + y(t)\sin\varphi_1 + \ell_1\theta_1(t) \\ \theta_2(t) \\ x(t)\cos\varphi_2 + y(t)\sin\varphi_2 + \ell_2\theta_2(t) \\ x(t)\sin\varphi_1 + y(t)\cos\varphi_1 \\ x(t)\sin\varphi_2 - y(t)\cos\varphi_2 \end{bmatrix} = \mathbf{C}^T \begin{bmatrix} x(t) \\ y(t) \\ \theta_1(t) \\ \theta_2(t) \end{bmatrix}. \tag{4}$$

2 THERMAL DYNAMICS

Following Thornton,[6] for each beam, the external heat flux in the space normal to the beam's surface is given by $S_i \doteq S_0 \cos\left(\xi_i - \frac{\partial w^i}{\partial s_i}\right)$, where S_0 is the solar flux and ξ_i is the angle of orientation of the solar vector with respect to beam i. Since $\frac{\partial w^i}{\partial s_i}$ is small, it is negligible. We denote by $T^i = T^i(t, s_i, \phi_i)$ the deviation of the temperature of beam i with respect to a reference temperature T_0^i. Then, conservation of energy for a small segment of circular cylinder including longitudinal and circumferential conduction in the cylinder wall and radiation from the cylinder's surface yields:

$$\rho_i c_i \frac{\partial T^i}{\partial t} - \frac{k_c^i}{R_i^2}\frac{\partial^2 T^i}{\partial \phi_i^2} - k_a^i \frac{\partial^2 T^i}{\partial s_i^2} + \frac{\sigma\epsilon_i}{h_i}(T_0^i + T^i)^4 = \frac{\alpha_s^i}{h_i} S_i \cos(\phi_i)\,\delta(\phi_i) \tag{5}$$

where k_a^i and k_c^i are the axial and circumferential thermal conductivity coefficients, respectively, c_i is the specific heat, R_i is the cylinder radius, h_i is the wall thickness, ϵ_i is the surface emissivity and α_s^i is the surface absorptivity, all of beam i, σ is the Stefan-Boltzmann constant, $\delta(\phi_i) = 1$ for $\phi_i \in (-\frac{\pi}{2}, \frac{\pi}{2})$, and $\delta(\phi_i) = 0$ for $\phi_i \in [-\pi, -\frac{\pi}{2}] \cup [\frac{\pi}{2}, \pi]$. The heat flux distribution on the RHS of equation (5) can be written as

$$S_i \cos(\phi_i)\,\delta(\phi_i) \;=\; S_i(\frac{1}{\pi} + g(\phi_i)) \;=\; \frac{S_i}{\pi} + S_i\, g(\phi_i) \tag{6}$$

where

$$g(\phi_i) = \begin{cases} \cos(\phi_i) - \frac{1}{\pi}, & \text{for } \phi_i \in [-\frac{\pi}{2}, \frac{\pi}{2}] \\ -\frac{1}{\pi}, & \text{for } \phi_i \in [-\pi, -\frac{\pi}{2}) \cup (\frac{\pi}{2}, \pi]. \end{cases}$$

Clearly $g(\phi_i)$ is continuous and it has zero average in $[-\pi, \pi]$.

For each beam, the temperature distribution is separated into two parts, namely:

$$T^i(t, s_i, \phi_i) = T^i(t, s_i) + T^{m,i}(t, s_i)\, g(\phi_i), \tag{7}$$

where $T^i(t,s_i)$ is independent of ϕ_i and corresponds to the uniform part of the flux, $\frac{S_i}{\pi}$, in (6), and $T^{m,i}(t,s_i)\,g(\phi_i)$ amounts for the circumferential variation of the flux in (6). Note that for every $s_i \in [0,L_i]$, $t \geq 0$ $T^{m,i}(t,s_i) = T^i(t,s_i,0) - T^i(t,s_i,\pi) \;=\; T^i(t,s_i,0) - T^i(t,s_i,\phi)$ for any $\phi \in [-\pi,-\frac{\pi}{2}) \cup (\frac{\pi}{2},\pi]$.

Also, we approximate the thermal radiation term $(T_0^i + T^i(t,s_i,\phi_i)\,)^4$ in (5) by linearizing $T(t,s_i,\phi_i)$ around $T(t,s_i,\phi_i) = T_s^i$ (where T_s^i, to be determined later, is the steady-state constant temperature increment produced on the undeformed beam i by the solar flux S_i), i.e., we approximate $(T_0^i+T^i(t,s_i,\phi_i)\,)^4$ by $(T_0^i+T_s^i)^4+4(T_0^i+T_s^i)^3\,(T^i(t,s_i) - T_s^i + T^{m,i}(t,s_i)g(\phi_i))$. Hence equation (5) is replaced by

$$\begin{aligned}
&\rho_i c_i \frac{\partial T^i(t,s_i)}{\partial t} + \rho_i c_i \frac{\partial T^{m,i}(t,s_i)}{\partial t}\, g(\phi_i) - \frac{k_c^i}{R_i^2} T^{m,i}(t,s_i)\, g''(\phi_i) \\
&- k_a^i \frac{\partial^2 T^i(t,s_i)}{\partial s_i^2} - k_a^i \frac{\partial^2 T^{m,i}(t,s_i)}{\partial s_i^2}\, g(\phi_i) \\
&+ \frac{\sigma\epsilon_i}{h_i}\left[(T_0^i + T_s^i)^4 + 4(T_0^i + T_s^i)^3\left(T^i(t,s_i) - T_s^i + T^{m,i}(t,s_i)g(\phi_i)\,\right)\right] \\
&= \frac{\alpha_s^i S_i}{h_i}\left[\frac{1}{\pi} + g(\phi_i)\right]
\end{aligned} \tag{8}$$

Integration of equation (8) over the cylinder's cross sectional area yields

$$\begin{aligned}
&\rho_i c_i \frac{\partial T^i(t,s_i)}{\partial t} - k_a^i \frac{\partial^2 T^i(t,s_i)}{\partial s_i^2} + \frac{4\sigma\epsilon_i (T_0^i + T_s^i)^3}{h_i}[T^i(t,s_i) - T_s^i] \\
&\quad = \left[\frac{\alpha_s^i S_i}{\pi h_i} - \frac{\sigma\epsilon_i (T_0^i + T_s^i)^4}{h_i}\right] \doteq f_i\,.
\end{aligned} \tag{9}$$

Next, note that in this equation, the temperature T_s^i is determined by setting the RHS, f_i, equals to zero. By doing so we obtain

$$T_s^i = \left(\frac{\alpha_s^i S_i}{\pi\sigma\epsilon_i}\right)^{\frac{1}{4}} - T_0^i \tag{10}$$

Note that with this value of T_s^i we have $T^i(t,s_i) = T_s^i$ at the steady-state and, since usually $T^{m,i}(t,s_i)$ is small compared to T_0^i, the linearization of the thermal radiation term performed above, is justified near the steady state solution.

Now multiplying equation (8) by $g(\phi_i)$ and integrating over the cylinder's cross sectional area, we obtain for $T^{m,i}$ the following equation:

$$\begin{aligned}
\rho_i c_i \|g\|^2 \frac{\partial T^{m,i}(t,s_i)}{\partial t} - k_a^i \frac{\partial^2 T^{m,i}(t,s_i)}{\partial s_i^2}\|g\|^2 - \frac{k_c^i}{R_i^2} T^{m,i}(t,s_i) \int_{-\pi}^{\pi} g''(\phi_i) g(\phi_i)\, d\phi_i \\
+ \frac{4\sigma\epsilon_i (T_0^i + T_s^i)^3}{h_i}\|g\|^2\, T^{m,i}(t,s_i) = \frac{\alpha_s^i S_i}{h_i}\|g\|^2.
\end{aligned}$$

Since $\|g\|^2 = \int_{-\pi}^{\pi} g(\phi_i)^2\, d\phi_i = \frac{\pi^2-4}{2\pi}$ and $\int_{-\pi}^{\pi} g''(\phi_i)g(\phi_i)\, d\phi_i = -\frac{\pi}{2}$, the equation above reads:

$$\rho_i c_i \frac{\partial T^{m,i}(t,s_i)}{\partial t} - k_a^i \frac{\partial^2 T^{m,i}(t,s_i)}{\partial s_i^2} + \left(\frac{k_c^i \pi^2}{R_i^2(\pi^2-4)} + \frac{4\sigma\epsilon_i (T_0^i + T_s^i)^3}{h_i} \right) T^{m,i}(t,s_i) = \frac{\alpha_s^i S_i}{h_i}. \tag{11}$$

To consider the thermally induced vibration in the system, we use Hooke's law for the stress-strain relation in the form of $\epsilon_{11}^i = \frac{1}{E_i}\sigma_{11}^i + \alpha_i T^i$, where α_i is the thermal expansion coefficient, and T^i is, as before, the deviation from the reference temperature T_0^i. Note that at $T^i = 0$ thermal strain vanishes, so that T_0^i is interpreted as the (uniform) temperature of beam i in the unstressed, rest-state. By the standard derivation of Euler-Bernoulli beam equation, we modify the Joint-Leg-Beam system (1) as follows:

$$\rho_i A_i \frac{\partial^2 u^i(t,s_i)}{\partial t^2} = E_i A_i \frac{\partial}{\partial s_i}\left(\frac{\partial u^i(t,s_i)}{\partial s_i} - \alpha_i T^i(t,s_i) \right), \tag{12}$$

$$\rho_i A_i \frac{\partial^2 w^i(t,s_i)}{\partial t^2} = -E_i I_i \frac{\partial^2}{\partial s_i^2}\left(\frac{\partial^2 w^i(t,s_i)}{\partial s_i^2} + \alpha_i T^{m,i}(t,s_i) \right) \tag{13}$$

The above beam equations are coupled to the heat equations modified from equations (9) and (11) and with T_s^i chosen as in equation (10) (so that $f_i = 0$ in (9)), that is:

$$\rho_i c_i \frac{\partial T^i(t,s_i)}{\partial t} = k_a^i \frac{\partial^2 T^i(t,s_i)}{\partial s_i^2} - \frac{4\sigma\epsilon_i (T_0^i + T_s^i)^3}{h_i}\left(T^i(t,s_i) - T_s^i \right) - \alpha_i E_i A_i T_0^i \frac{\partial^2}{\partial s_i \partial t} u^i(t,s_i)\ , \tag{14}$$

and

$$\rho_i c_i \frac{\partial T^{m,i}(t,s_i)}{\partial t} = k_a^i \frac{\partial^2 T^{m,i}(t,s_i)}{\partial s_i^2} - \left[\frac{k_c^i \pi^2}{R_i^2(\pi^2-4)} + \frac{4\sigma\epsilon_i (T_0^i + T_s^i)^3}{h_i} \right] T^{m,i}(t,s_i) + \alpha_i E_i I_i T_0^i \frac{\partial^3}{\partial s_i^2 \partial t} w^i(t,s_i) + \frac{\alpha_s^i S_i}{h_i}, \tag{15}$$

We impose Robin type boundary conditions for the temperature at both ends of each beam, i.e. $\frac{\partial}{\partial s_i} T^i(t,s_i,\phi_i)\mid_{s_i=L_i} = \lambda_R^i \left(T^* - T_0^i - T^i(t,L_i,\phi_i) \right)$, $\frac{\partial}{\partial s_i} T^i(t,s_i,\phi_i)\mid_{s_i=0} = \lambda_L^i (T_0^i + T^i(t,0,\phi_i) - T^*)$, $\forall t \geq 0,\ \phi_i \in [-\pi,\pi],\ i = 1,2$, where T^* is the temperature of the surrounding medium and λ_L^i, λ_R^i, $i = 1,2$, are nonnegative constants. By writing $T^i(t,s_i,\phi_i)$ in terms of the decomposition given in (7) these equations take the form:

$$\frac{\partial}{\partial s_i} T^i(t,L_i) + \frac{\partial}{\partial s_i} T^{m,i}(t,L_i) g(\phi_i) = \lambda_R^i \left(T^* - T_0^i - T^i(t,L_i) - T^{m,i}(t,L_i) g(\phi_i) \right),$$

$$\frac{\partial}{\partial s_i} T^i(t,0) + \frac{\partial}{\partial s_i} T^{m,i}(t,0) g(\phi_i) = \lambda_L^i \left(T_0^i + T^i(t,0) + T^{m,i}(t,0) g(\phi_i) - T^* \right).$$

Since these equations must hold for all $\phi_i \in [-\pi, \pi]$ it follows that

$$\frac{\partial}{\partial s_i}T^i(t,L_i) = \lambda_R^i\left(T^* - T_0^i - T^i(t,L_i)\right), \quad \frac{\partial}{\partial s_i}T^i(t,0) = \lambda_L^i\left(T_0^i + T^i(t,0) - T^*\right) \tag{16}$$

and

$$\frac{\partial}{\partial s_i}T^{m,i}(t,L_i) = -\lambda_R^i T^{m,i}(t,L_i), \quad \frac{\partial}{\partial s_i}T^{m,i}(t,0) = \lambda_L^i T^{m,i}(t,0), \tag{17}$$

for all $t \geq 0$, $i = 1, 2$. So, just like the dynamics for the temperature distribution (8) decouples into equations (14) and (15) for T^i and $T^{m,i}$, respectively, we observe that the boundary conditions also decouple. Note however in equation (16) that the boundary conditions for the axial component of the temperature, $T^i(t, s_i)$, are non-homogeneous. By defining $\tilde{T^i}(t, s_i) \doteq T^i(t, s_i) - (T^* - T_0^i)$, equation (14) can be written in the form

$$\begin{aligned}\rho_i c_i \frac{\partial \tilde{T^i}(t,s_i)}{\partial t} &= k_a^i \frac{\partial^2 \tilde{T^i}(t,s_i)}{\partial s_i^2} - \frac{4\sigma\epsilon_i (T_0^i + T_s^i)^3}{h_i}\left(\tilde{T^i}(t,s_i) + T^* - T_0^i - T_s^i\right) \\ &- \alpha_i E_i A_i T_0^i \frac{\partial^2}{\partial s_i \partial t} u^i(t,s_i)\ ,\end{aligned} \tag{18}$$

while the boundary conditions (16) now take the form

$$\frac{\partial}{\partial s_i}\tilde{T^i}(t,L_i) = -\lambda_R^i \tilde{T^i}(t,L_i), \quad \frac{\partial}{\partial s_i}\tilde{T^i}(t,0) = \lambda_L^i \tilde{T^i}(t,0), \tag{19}$$

Observe now that these boundary conditions are exactly the same as those in (17) for the circumferential component of the temperature. Finally, note also that in equation (12), $T^i(t, s_i)$ can be replaced by $\tilde{T^i}(t, s_i)$ without any changes.

System (12)-(15) (or equivalently (12), (13), (15), (18)), together with the joint-leg dynamics described by equation (1) constitute the thermoelastic Joint-Leg-Beam equations with the external solar heat source. The extensional forces, shear forces and bending moments of the beams at $s_i = L_i$ are now given by:

$$F_i(t) = E_i A_i \left(\frac{\partial u^i}{\partial s_i}(t,s_i) - \alpha_i T^i(t,s_i)\right)\Big|_{s_i=L_i} \tag{20}$$

$$N_i(t) = E_i I_i \frac{\partial}{\partial s_i}\left(\frac{\partial^2 w^i}{\partial s_i^2}(t,s_i) + \alpha_i T^{m,i}(t,s_i)\right)\Big|_{s_i=L_i}, \tag{21}$$

$$M_i(t) = E_i I_i \left(\frac{\partial^2 w^i}{\partial s_i^2}(t,s_i) + \alpha_i T^{m,i}(t,s_i)\right)\Big|_{s_i=L_i}. \tag{22}$$

A state-space formulation and semigroup theory can be used to establish well-posedness and exponential stability of this system. We refer the reader to Cliff et all[3] for details on this issues. In what follows we characterize the equilibrium solutions and present several numerical results.

3 EQUILIBRIUM STATE

The equilibrium state, or time-invariant solution, is characterized by equations (12) - (15) with time-derivatives set to zero. From those equations we find that

$$\begin{aligned}
\frac{\partial}{\partial s_i} u^i(s_i) &= \alpha_i T^i(s_i) + C_i \ , && (23)\\
\frac{\partial^2}{\partial s_i^2} w^i(s_i) &= -\alpha_i T^{m,i}(s_i) + D_1^i s_i + D_2^i \ , && (24)\\
T^i(s_i) &= T_s^i + E_1^i \cosh(\beta_i s_i) + E_2^i \sinh(\beta_i s_i) \ , && (25)\\
T^{m,i}(s_i) &= \frac{\alpha_s^i S_i}{k_a^i h_i \delta_i^2} + F_1^i \cosh(\delta_i s_i) + F_2^i \sinh(\delta_i s_i) \ , && (26)
\end{aligned}$$

where $\beta_i \doteq \sqrt{\frac{4\sigma\epsilon_i (T_0^i + T_s^i)^3}{h_i k_a^i}}$, $\delta_i \doteq \sqrt{\frac{\pi^2 k_c^i}{k_a^i R_i^2(\pi^2-4)} + \frac{4\sigma\epsilon_i (T_0^i+T_s^i)^3}{k_a^i h_i}}$ and C_i, D_j^i, E_j^i, F_j^i, $i,j = 1,2$, are constants to be determined using the boundary conditions.

Specifically, from equations (25) and (26) and the boundary conditions (16), (17), we obtain:

$$\begin{aligned}
&E_1^i \left(\beta_i \sinh(\beta_i L_i) + \lambda_R^i \cosh(\beta_i L_i)\right) + E_2^i \left(\beta_i \cosh(\beta_i L_i) + \lambda_R^i \sinh(\beta_i L_i)\right)\\
&\qquad = \lambda_R^i (T^* - T_0^i - T_s^i),\\
&E_1^i \lambda_L^i - E_2^i \beta_i = \lambda_L^i (T^* - T_0^i - T_s^i),
\end{aligned}$$

and

$$\begin{aligned}
&F_1^i \left(\delta_i \sinh(\delta_i L_i) + \lambda_R^i \cosh(\delta_i L_i)\right) + F_2^i \left(\delta_i \cosh(\delta_i L_i) + \lambda_R^i \sinh(\delta_i L_i)\right)\\
&\qquad = -\lambda_R^i \nu_i,\\
&F_1^i \lambda_L^i - F_2^i \delta_i = -\lambda_L^i \nu_i,
\end{aligned}$$

where $\nu_i \doteq \frac{\alpha_s^i S_i}{k_a^i h_i \delta_i^2}$. Solving these two systems of equations we obtain:

$$\begin{aligned}
E_1^i &= \frac{(T^* - T_0^i - T_s^i)\,(\beta_i \lambda_R^i + \beta_i \lambda_L^i \cosh(\beta_i L_i) + \lambda_L^i \lambda_R^i \sinh(\beta_i L_i))}{\beta_i(\lambda_L^i + \lambda_R^i)\cosh(\beta_i L_i) + (\beta_i^2 + \lambda_L^i \lambda_R^i)\sinh(\beta_i L_i)},\\
E_2^i &= \frac{(T^* - T_0^i - T_s^i)\,(\lambda_L^i \lambda_R^i (1 - \cosh(\beta_i L_i)) - \beta_i \lambda_L^i \sinh(\beta_i L_i))}{\beta_i(\lambda_L^i + \lambda_R^i)\cosh(\beta_i L_i) + (\beta_i^2 + \lambda_L^i \lambda_R^i)\sinh(\beta_i L_i)},\\
F_1^i &= \frac{-\nu_i\,(\delta_i \lambda_R^i + \delta_i \lambda_L^i \cosh(\delta_i L_i) + \lambda_L^i \lambda_R^i \sinh(\delta_i L_i))}{(\delta_i^2 + \lambda_L^i \lambda_R^i)\sinh(\delta_i L_i) + \delta_i(\lambda_L^i + \lambda_R^i)\cosh(\delta_i L_i)},\\
F_2^i &= \frac{\nu_i\,(\delta_i \lambda_L^i \sinh(\delta_i L_i) + \lambda_L^i \lambda_R^i \cosh(\delta_i L_i) - \lambda_L^i \lambda_R^i)}{(\delta_i^2 + \lambda_L^i \lambda_R^i)\sinh(\delta_i L_i) + \delta_i(\lambda_L^i + \lambda_R^i)\cosh(\delta_i L_i)}, \quad i = 1,2. \qquad (27)
\end{aligned}$$

Replacing now these known steady-state temperature profiles (25)-(26) into (23)-(24) and

using the boundary conditions (3) we obtain

$$u^i(s_i) \;=\; (\alpha_i T_s^i + C_i)\, s_i + \frac{\alpha_i E_1^i}{\beta_i}\sinh(\beta_i s_i) + \frac{\alpha_i E_2^i}{\beta_i}\left(\cosh(\beta_i s_i) - 1\right)\;, \tag{28}$$

$$\begin{aligned} w^i(s_i) \;=\; & \frac{D_1^i}{6}\, s_i^3 + \frac{D_2^i - \alpha_i \nu_i}{2}\, s_i^2 - \frac{\alpha_i F_1^i}{\delta_i^2}\left(\cosh(\delta_i s_i) - 1\right) \\ & - \frac{\alpha_i F_2^i}{\delta_i^2}\left(\sinh(\delta_i s_i) - \delta_i s_i\right)\;. \end{aligned} \tag{29}$$

The constants C_i, D_1^i, D_2^i, $i = 1, 2$, in (28)-(29) must now be determined using the dynamic and geometric compatibility conditions at $s_i = L_i$. The steady state version of the joint-legs equations (1) lead to

$$\ell_i N_i + M_i = 0\;, \quad i = 1, 2\;, \tag{30}$$

and

$$\begin{bmatrix} \sin\varphi_1 & -\cos\varphi_1 \\ \cos\varphi_1 & \sin\varphi_1 \end{bmatrix} \begin{bmatrix} F_1 \\ N_1 \end{bmatrix} + \begin{bmatrix} \sin\varphi_2 & \cos\varphi_2 \\ -\cos\varphi_2 & \sin\varphi_2 \end{bmatrix} \begin{bmatrix} F_2 \\ N_2 \end{bmatrix} = \begin{bmatrix} 0 \\ 0 \end{bmatrix}\;. \tag{31}$$

Replacing with (26) and (29) into (21) and (22) we obtain that $M_i = E_i I_i (D_1^i\, L_i + D_2^i)$ and $N_i = E_i I_i\, D_1^i$. Substituting into the equation (30) above we then obtain that

$$D_2^i = -(\ell_i + L_i)\, D_1^i, \;\; i = 1, 2\;. \tag{32}$$

This reduces to four the number of constants to be determined in (28)-(29), namely C_1, C_2, D_1^1 and D_1^2. Also, replacing with (25) and (28) into (20) we obtain that

$$F_i \;=\; E_i\, A_i\, C_i, \quad i = 1, 2.$$

Hence, equation (31) takes the form

$$C_1 E_1 A_1 \sin\varphi_1 + C_2 E_2 A_2 \sin\varphi_2 - D_1^1 E_1 I_1 \cos\varphi_1 + D_1^2 E_2 I_2 \cos\varphi_2 \;=\; 0 \tag{33}$$

$$C_1 E_1 A_1 \cos\varphi_1 - C_2 E_2 A_2 \cos\varphi_2 + D_1^1 E_1 I_1 \sin\varphi_1 + D_1^2 E_2 I_2 \sin\varphi_2 \;=\; 0 \tag{34}$$

These are the first two equations needed to determine C_1, C_2, D_1^1 and D_1^2. The other two will come from the geometric compatibility conditions at the leg-beam interfaces. These conditions require (see[1]) that for every $t \geq 0$:

$$\begin{aligned} & \ell_1 w_{s_1}^1(t, L_1)\cos\varphi_1 + w^1(t, L_1)\cos\varphi_1 + u^1(t, L_1)\sin\varphi_1 \\ & \;=\; \ell_2 w_{s_2}^2(t, L_2)\cos\varphi_2 + w^2(t, L_2)\cos\varphi_2 + u^2(t, L_2)\sin\varphi_2 \end{aligned} \tag{35}$$

and

$$\begin{aligned} & \ell_1 w_{s_1}^1(t, L_1)\sin\varphi_1 + w^1(t, L_1)\sin\varphi_1 - u^1(t, L_1)\cos\varphi_1 \\ & = -\ell_2 w_{s_2}^2(t, L_2)\sin\varphi_2 - w^2(t, L_2)\sin\varphi_2 + u^2(t, L_2)\cos\varphi_2 \end{aligned} \tag{36}$$

In particular, using (28), (29) and replacing D_2^1 and D_2^2 by (32), we find that at the steady-state, the above two geometric compatibility conditions can be written in the form:

$$\begin{aligned} & C_1 L_1 \sin\varphi_1 - C_2 L_2 \sin\varphi_2 - D_1^1 L_1 \cos\varphi_1 \left(\ell_1^2 + \ell_1 L_1 + \frac{L_1^2}{3}\right) + D_1^2 L_2 \cos\varphi_2 \left(\ell_2^2 + \ell_2 L_2 + \frac{L_2^2}{3}\right) \\ &= \sum_{i=1}^{2} (-1)^{i+1} \left[\ell_i \cos\varphi_i \left(\alpha_i \nu_i L_i + \frac{\alpha_i F_1^i}{\delta_i} \sinh(\delta_i L_i) + \frac{\alpha_i F_2^i}{\delta_i} (\cosh(\delta_i L_i) - 1) \right) \right. \\ &\quad + \cos\varphi_i \left(\frac{\alpha_i \nu_i L_i^2}{2} + \frac{\alpha_i F_1^i}{\delta_i^2} (\cosh(\delta_i L_i) - 1) + \frac{\alpha_i F_2^i}{\delta_i^2} (\sinh(\delta_i L_i) - \delta_i L_i) \right) \\ &\quad \left. - \sin\varphi_i \left(\alpha_i T_s^i L_i + \frac{\alpha_i E_1^i}{\beta_i} \sinh(\beta_i L_i) + \frac{\alpha_i E_2^i}{\beta_i} (\cosh(\beta_i L_i) - 1) \right) \right], \end{aligned} \tag{37}$$

and

$$\begin{aligned} & C_1 L_1 \cos\varphi_1 + C_2 L_2 \cos\varphi_2 + D_1^1 L_1 \sin\varphi_1 \left(\ell_1^2 + \ell_1 L_1 + \frac{L_1^2}{3}\right) + D_1^2 L_2 \sin\varphi_2 \left(\ell_2^2 + \ell_2 L_2 + \frac{L_2^2}{3}\right) \\ &= -\sum_{i=1}^{2} \left[\ell_i \sin\varphi_i \left(\alpha_i \nu_i L_i + \frac{\alpha_i F_1^i}{\delta_i} \sinh(\delta_i L_i) + \frac{\alpha_i F_2^i}{\delta_i} (\cosh(\delta_i L_i) - 1) \right) \right. \\ &\quad + \sin\varphi_i \left(\frac{\alpha_i \nu_i L_i^2}{2} + \frac{\alpha_i F_1^i}{\delta_i^2} (\cosh(\delta_i L_i) - 1) + \frac{\alpha_i F_2^i}{\delta_i^2} (\sinh(\delta_i L_i) - \delta_i L_i) \right) \\ &\quad \left. + \cos\varphi_i \left(\alpha_i T_s^i L_i + \frac{\alpha_i E_1^i}{\beta_i} \sinh(\beta_i L_i) + \frac{\alpha_i E_2^i}{\beta_i} (\cosh(\beta_i L_i) - 1) \right) \right], \end{aligned} \tag{38}$$

The four equations (33)-(34)-(37)-(38) uniquely determine the four constants C_1, C_2, D_1^1 and D_1^2.

Summarizing, the steady-state solutions of the thermoelastic joint-leg-beam equations (12)-(15), (1), with the boundary conditions (3), (16), (17), extensional forces, shear forces and bending moments at the right endpoints of the beams given by equations (20)-(22) and geometric compatibility conditions at the beam-leg interfaces given by (35)-(36), are given by:

$$\begin{aligned} u^i(s_i) &= (\alpha_i T_s^i + C_i)\, s_i + \frac{\alpha_i E_1^i}{\beta_i} \sinh(\beta_i s_i) + \frac{\alpha_i E_2^i}{\beta_i} (\cosh(\beta_i s_i) - 1) \ , \\ w^i(s_i) &= \frac{D_1^i}{6}\, s_i^3 + \frac{D_2^i - \alpha_i \nu_i}{2}\, s_i^2 - \frac{\alpha_i F_1^i}{\delta_i^2} (\cosh(\delta_i s_i) - 1) - \frac{\alpha_i F_2^i}{\delta_i^2} (\sinh(\delta_i s_i) - \delta_i s_i) \ . \end{aligned}$$

where

$$\begin{aligned} & T_s^i = \left(\frac{\alpha_s^i S_i}{\pi \sigma \epsilon_i} \right)^{\frac{1}{4}} - T_0^i, \qquad \nu_i = \frac{\alpha_s^i S_i}{k_a^i h_i \delta_i^2}, \\ & \beta_i = \sqrt{\frac{4\sigma\epsilon_i (T_0^i + T_s^i)^3}{h_i k_a^i}}, \quad \delta_i = \sqrt{\frac{\pi^2 k_c^i}{k_a^i R_i^2 (\pi^2 - 4)} + \frac{4\sigma\epsilon_i (T_0^i + T_s^i)^3}{k_a^i h_i}}, \end{aligned}$$

E_j^i, F_j^i, $i,j = 1,2$, are as given in (27), the four constants C_1, C_2, D_1^1, D_1^2 are the solutions of the equation $A \begin{pmatrix} C_1 \\ C_2 \\ D_1^1 \\ D_1^2 \end{pmatrix} = Y$ where

$$A = \begin{pmatrix} E_1 A_1 \sin\varphi_1 & E_2 A_2 \sin\varphi_2 & -E_1 I_1 \cos\varphi_1 & E_2 I_2 \cos\varphi_2 \\ E_1 A_1 \cos\varphi_1 & -E_2 A_2 \cos\varphi_2 & E_1 I_1 \sin\varphi_1 & E_2 I_2 \sin\varphi_2 \\ L_1 \sin\varphi_1 & -L_2 \sin\varphi_2 & -L_1(\ell_1^2+\ell_1 L_1+\frac{L_1^2}{3})\cos\varphi_1 & L_2(\ell_2^2+\ell_2 L_2+\frac{L_2^2}{3})\cos\varphi_2 \\ L_1 \cos\varphi_1 & L_2 \cos\varphi_2 & L_1(\ell_1^2+\ell_1 L_1+\frac{L_1^2}{3})\sin\varphi_1 & L_2(\ell_2^2+\ell_2 L_2+\frac{L_2^2}{3})\sin\varphi_2 \end{pmatrix}, \quad Y = \begin{pmatrix} 0 \\ 0 \\ y_3 \\ y_4 \end{pmatrix},$$

with

$$\begin{aligned} y_3 = & \sum_{i=1}^{2}(-1)^{i+1}\left[\ell_i \cos\varphi_i \left(\alpha_i \nu_i L_i + \frac{\alpha_i F_1^i}{\delta_i}\sinh(\delta_i L_i) + \frac{\alpha_i F_2^i}{\delta_i}(\cosh(\delta_i L_i)-1)\right)\right. \\ & + \cos\varphi_i \left(\frac{\alpha_i \nu_i L_i^2}{2} + \frac{\alpha_i F_1^i}{\delta_i^2}(\cosh(\delta_i L_i)-1) + \frac{\alpha_i F_2^i}{\delta_i^2}(\sinh(\delta_i L_i)-\delta_i L_i)\right) \\ & \left. - \sin\varphi_i \left(\alpha_i T_s^i L_i + \frac{\alpha_i E_1^i}{\beta_i}\sinh(\beta_i L_i) + \frac{\alpha_i E_2^i}{\beta_i}(\cosh(\beta_i L_i)-1)\right)\right], \\ y_4 = & -\sum_{i=1}^{2}\left[\ell_i \sin\varphi_i \left(\alpha_i \nu_i L_i + \frac{\alpha_i F_1^i}{\delta_i}\sinh(\delta_i L_i) + \frac{\alpha_i F_2^i}{\delta_i}(\cosh(\delta_i L_i)-1)\right)\right. \\ & + \sin\varphi_i \left(\frac{\alpha_i \nu_i L_i^2}{2} + \frac{\alpha_i F_1^i}{\delta_i^2}(\cosh(\delta_i L_i)-1) + \frac{\alpha_i F_2^i}{\delta_i^2}(\sinh(\delta_i L_i)-\delta_i L_i)\right) \\ & \left. + \cos\varphi_i \left(\alpha_i T_s^i L_i + \frac{\alpha_i E_1^i}{\beta_i}\sinh(\beta_i L_i) + \frac{\alpha_i E_2^i}{\beta_i}(\cosh(\beta_i L_i)-1)\right)\right], \end{aligned}$$

and finally the two constants D_2^1, D_2^2 are given by $D_2^i = -(\ell_i + L_i)\, D_1^i, \quad i = 1,2.$

4 NUMERICAL RESULTS

We now present some numerical results for the thermal steady-state deflections of the two beams in our joint-leg-beam system, after they are subjected to a solar radiation flux acting on different angles. The values used for these simulations are shown in Table 1 and correspond to a composite material. The mass of each leg was set equal to 8% of the mass of each beam and the mass of the joint's tip was taken equal to 4% of the beam's mass.

Note that with the values of φ_1 and φ_2 given in Table 1, the angle between both beams is $\pi/2$. Thus, for instance, a perpendicular solar flux on one of the beams will have no thermal effect on the other.

4.1 Case 1: No flux at the boundaries: $\lambda_L^1 = \lambda_R^1 = \lambda_L^2 = \lambda_R^2 = 0$

Experiment 1: $\xi_1 = 0$**,** $\xi_2 = \frac{\pi}{2}$. Figure 3 shows the steady-state thermal transverse and mechanical axial deflections induced on both beams. The steady-state values for the axial and circumferential temperature deviations were: $T_s^1 = 16.1939$, $T_s^2 = -280$ (corresponding to temperatures of $296.1939\ K^{\circ}$ and $0\ K^{\circ}$, respectively), $\hat{T}^{m,1} = 207.2897\ K^{\circ}$ and $\hat{T}^{m,2} = 0\ K^{\circ}$. Steady-state temperatures of beam 1 are much

Table 1: Joint, legs, beams and solar radiation parameters

Parameter	Notation	Value
Beam's length	$L_1 = L_2$	2.00 m
Beam's radius	$R_1 = R_2$	0.064 m
Beam's thickness	$h_1 = h_2$	0.0003 m
Material density	$\rho_1 = \rho_2$	1320 $\mathrm{kg/m^3}$
Young's modulus	$E_1 = E_2$	0.9×10^{11} $\mathrm{N/m^2}$
Leg's length	$\ell_1 = \ell_2$	0.20 m (=$L_1/10$)
Leg's mass	$m_1 = m_2$	8 % mass of beam.
Joint's mass	m_p	4 % mass of beam.
Initial leg's angles	$\varphi_1 = \varphi_2$	$\pi/4$
Solar radiation	S_0	$1.37 \times\ 10^3$ $\mathrm{W/m^2}$
Stefan-Boltzman's constant	σ	$5.67 \times\ 10^{-8}$ $\mathrm{W/m^2\,K^4}$
Beam's surface (radiation) emissivity	$\epsilon_1 = \epsilon_2$	0.4
Beam's surface (radiation) absorsivity	$\alpha_s^1 = \alpha_s^2$	0.4
Beam's axial thermal conductivity	$k_a^1 = k_a^2$	5.75 $\mathrm{W/m\,K}$
Beam's circumferential thermal conductivity	$k_c^1 = k_c^2$	2.34 $\mathrm{W/m\,K}$
Undeformed reference temperature	$T_0^1 = T_0^2$	280 K
Thermal expansion coefficients	$\alpha_1 = \alpha_2$	1.0×10^{-6}

higher than those of beam 2 due to the fact that solar radiation is acting perpendicular to beam 1 and, therefore, parallel to beam 2. In Figure 3 we observe a negative thermal transverse bending in beam 1 and almost no transverse bending in beam 2. However, we observe that this transverse bending induces a mechanical (linear) compression in beam 2 due to the fact that the beams are coupled by the joint. Figure 4 shows the steady-state circumferential distribution of the temperature in both beams.

Experiment 2: $\xi_1 = -\frac{\pi}{2}$**,** $\xi_2 = 0$. This case is symmetric with respect to case 1. Solar radiation is now perpendicular to beam 2 and therefore, parallel to beam 1. Figure 5 shows the thermal transverse and mechanical axial deflections induced on both beams. The steady-state values for the axial and circumferential temperature deviations were: $T_s^1 = -280$, $T_s^2 = 16.1939$ (corresponding to temperatures of 0 K$^{\mathrm{o}}$ and 296.1939 K$^{\mathrm{o}}$, respectively), $\hat{T}^{m,1} = 0\ K^{\mathrm{o}}$ and $\hat{T}^{m,2} = 207.2897\ K^{\mathrm{o}}$. Figure 5 shows a negative thermal transverse bending in beam 2 and almost no transverse bending in beam 1. However, we observe that this thermal bending induces a mechanical (linear) compression in beam 1 due to the fact that the beams are coupled at the joint. Figure 6 shows the steady-state circumferential distribution of the temperature in both beams.

Experiment 3: $\xi_1 = -\frac{\pi}{4}$**,** $\xi_2 = \frac{\pi}{4}$. In this case the magnitude of the incident solar radiation angle is the same for both beams. Figure 7 shows the transverse and axial thermal deflections induced on both beams. The coupling of the joint produces a small (note the scale) positive transverse deflection near the right end of both beams while both remain in compression. The steady-state values were equal in both beams: $T_s^1 = T_s^2 = -8.3890$ (corresponding to a temperature of $271.6110\ K^{\mathrm{o}}$) and $\hat{T}^{m,1} = \hat{T}^{m,2} = 184.1316\ K^{\mathrm{o}}$. Figure 7 shows the transverse bending for both beams and a small linear compression in both beams due to the coupling produced by the joint. Figure 8 shows the steady-state circumferential

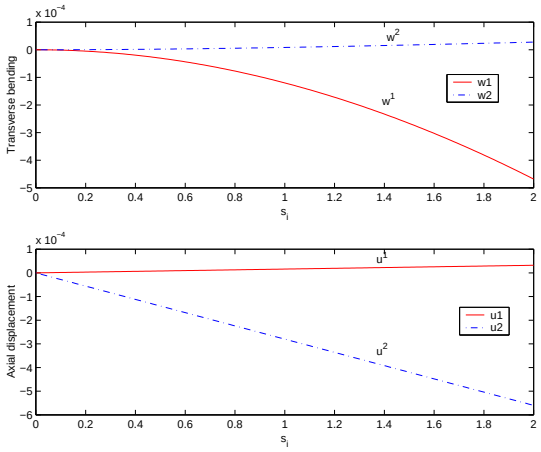

Figure 3: Steady-state thermal deflections for $\xi_1 = 0$, $\xi_2 = \frac{\pi}{2}$

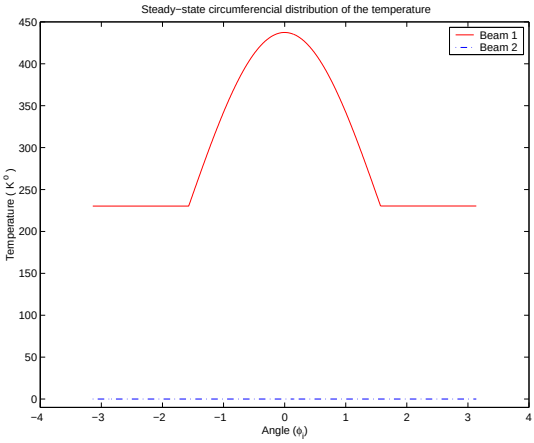

Figure 4: Steady-state circumferential temp. distribution, $\xi_1 = 0, \xi_2 = \frac{\pi}{2}$

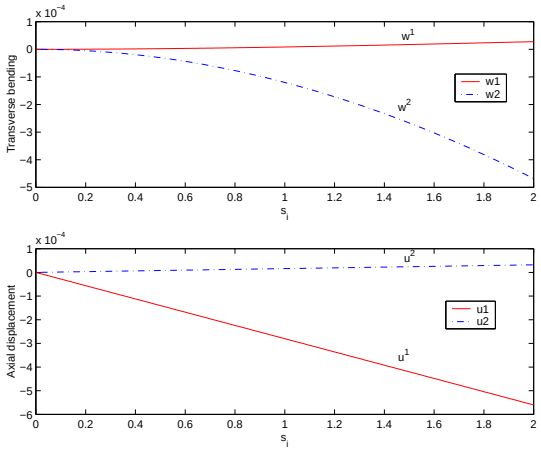

Figure 5: Steady-state thermal deflections for for $\xi_1 = -\frac{\pi}{2}$, $\xi_2 = 0$

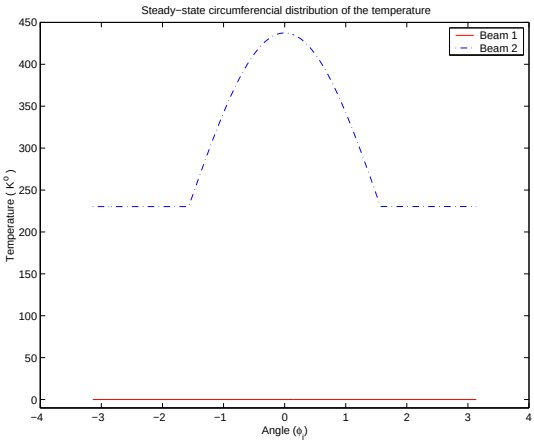

Figure 6: Steady-state circumferential temp. distrib., $\xi_1 = -\frac{\pi}{2}$, $\xi_2 = 0$

distribution of the temperature in both beams.

4.2 Case 2: With flux at some of the boundaries

Experiment 4: In this case we took again $\xi_1 = 0$, $\xi_2 = \frac{\pi}{2}$ just like in Experiment 1, so that the solar radiation is perpendicular to beam 1. Figure 9 shows the temperature distribution along beam 1 for the case of zero flux. For this case we saw that $T_s^1 = 16.1939\ K^o$. This is the value of the average steady-state temperature increment produced on beam 1 by the solar radiation. Therefore the steady-state average temperature of beam 1 is $T_0^1 + T_s^1 = 296.1939\ K^o$.

We then took $T^* = 296.1939\ K^o$, i.e. the external temperature was assumed to be equal to the average temperature of beam 1. We also took $\lambda_L^1 = 10$ and $\lambda_R^1 = \lambda_L^2 = \lambda_R^2 = 0$. Figure 10 shows the temperature distribution on beam 1 for this case. At the left boundary ($s_1 = 0$) we observe a temperature drop at the top part of the beam ($\phi_1 \approx 0$) and a temperature increase at the bottom ($\phi_1 \approx \pm\pi$). This

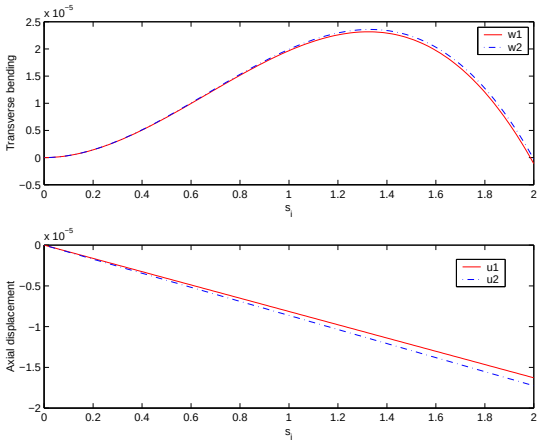

Figure 7: Steady-state thermal deflections for for $\xi_1 = -\frac{\pi}{4}$, $\xi_2 = \frac{\pi}{4}$

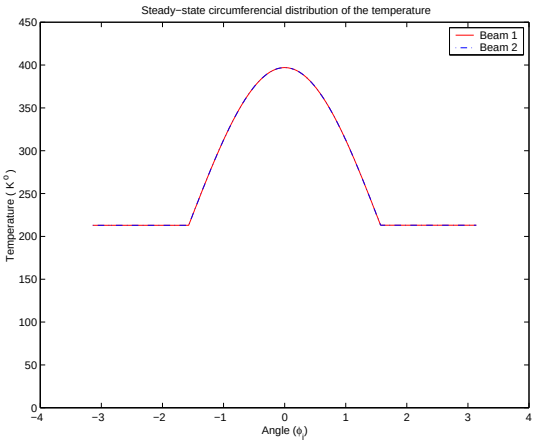

Figure 8: Steady-state circumferential temp. distrib., $\xi_1 = -\frac{\pi}{4}$, $\xi_2 = \frac{\pi}{4}$

is so because the upper part of the beam is hotter than the external temperature while the lower part is cooler. Figure 11 shows the steady-state transverse and axial deflections induced on both beams for this case. We observe no substantial differences with respect to the results obtained for the no-flux case (Experiment 1). This is justified because although heat is flowing out of the upper part of the left end of beam 1, the same amount is flowing in at the bottom, so keeping unchanged the average temperature of the beam. Figure 12 shows the circumferential temperature gradient $T^{m,1}(s_1)$ for this case. We see that its values are much smaller near the left boundary due to the fact that the flux here tends to make equal the temperatures at the top and bottom of the beam. In fact, $T^{m,1}(s_1)$ tends to zero at $s_1 = 0$ as the coefficient λ_L^1 increases.

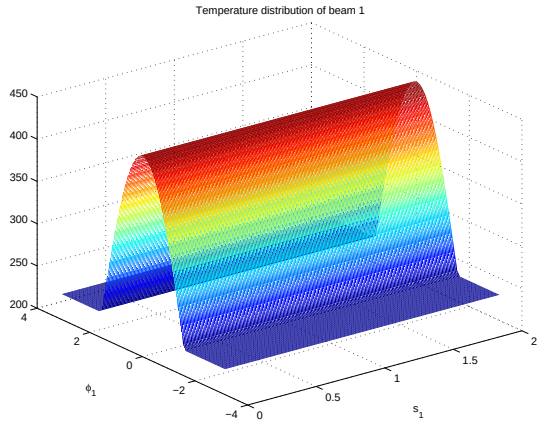

Figure 9: Temperature distribution on beam 1, $\xi_1 = 0$, $\xi_2 = \frac{\pi}{2}$, no boundary flux

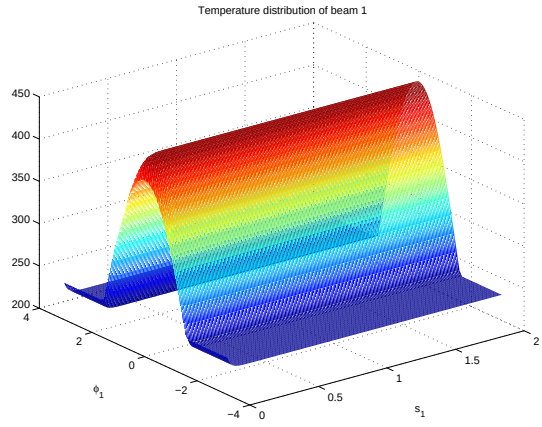

Figure 10: Temperature distribution on beam 1, $\xi_1 = 0$, $\xi_2 = \frac{\pi}{2}$, $T^* = T_0^1 + T_s^1 = 296.1939\ K^o$, $\lambda_L^1 = 10$, $\lambda_R^1 = \lambda_L^2 = \lambda_R^2 = 0$

Experiment 5: Same as in Experiment 4, except that now we took $T^* = 300\ K^o$, i.e. the external temperature is a few degrees above the average temperature of the beam. Also we chose $\lambda_L^1 = 100$ and

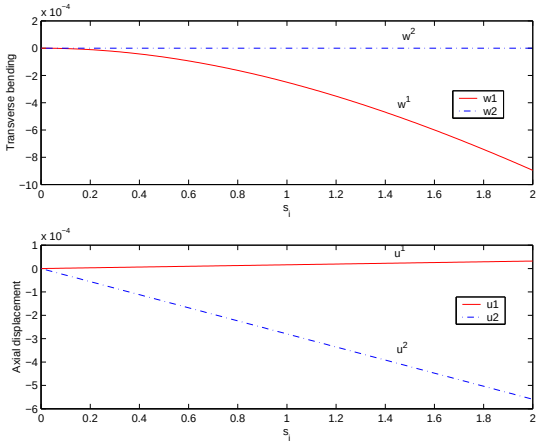

Figure 11: Transverse and axial deflections of beam 1, $\xi_1 = 0$, $\xi_2 = \frac{\pi}{2}$, $T^* = T_0^1 + T_s^1 = 296.1939\ K^o$, $\lambda_L^1 = 10$, $\lambda_R^1 = \lambda_L^2 = \lambda_R^2 = 0$

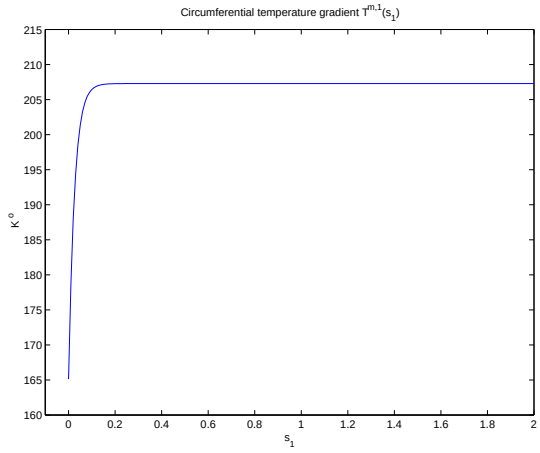

Figure 12: Circumferential temperature gradient, $T^{m,1}(s_1)$, $\xi_1 = 0$, $\xi_2 = \frac{\pi}{2}$, $T^* = T_0^1 + T_s^1 = 296.1939\ K^o$, $\lambda_L^1 = 10$, $\lambda_R^1 = \lambda_L^2 = \lambda_R^2 = 0$

$\lambda_R^1 = \lambda_L^2 = \lambda_R^2 = 0$. Once again, no significant changes are observed on the longitudinal and transverse deflection of the beams. Figure 13 show the transverse deflections and axial displacements in this case while Figure 14 depicts the temperature distribution on beam 1.

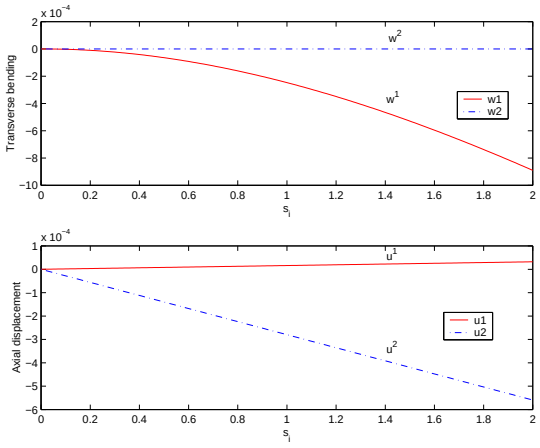

Figure 13: Transverse and axial deflections of beam 1, $\xi_1 = 0$, $\xi_2 = \frac{\pi}{2}$, $T^* = 300\ K^o$, $\lambda_L^1 = 100$, $\lambda_R^1 = \lambda_L^2 = \lambda_R^2 = 0$

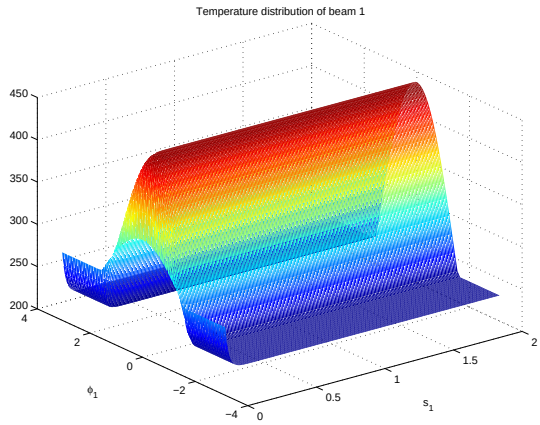

Figure 14: Temperature distribution on beam 1, $\xi_1 = 0$, $\xi_2 = \frac{\pi}{2}$, $T^* = 300\ K^o$, $\lambda_L^1 = 100$, $\lambda_R^1 = \lambda_L^2 = \lambda_R^2 = 0$

Experiment 6: Same as in Experiment 5, except that now we took $T^* = 290\ K^o$, i.e. the external temperature is a few degrees below the average temperature of the beam. Once again no significant changes are observed on the axial and transverse deflection of the beams. Figure 15 show the transverse deflections and axial displacements in this case while Figure 16 depicts the temperature distribution on beam 1.

Experiment 7: For this experiment we took $\xi_1 = -\frac{\pi}{4}$, $\xi_2 = \frac{\pi}{4}$, so that the solar incident angle is equal for both beams. Also we chose $T^* = 200\ K^o$, i.e. the external temperature is much smaller than

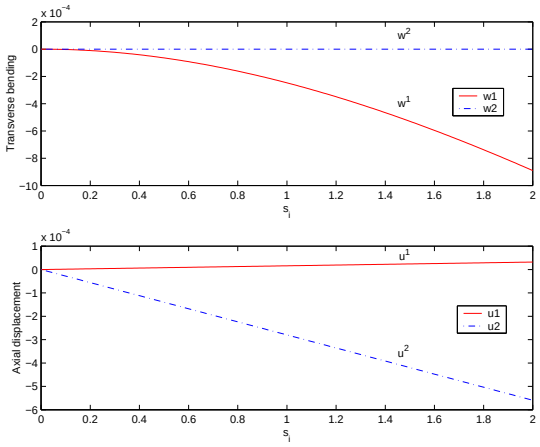

Figure 15: Transverse and axial deflections of beam 1, $\xi_1 = 0$, $\xi_2 = \frac{\pi}{2}$, $T^* = 290\ K^o$, $\lambda_L^1 = 100$, $\lambda_R^1 = \lambda_L^2 = \lambda_R^2 = 0$

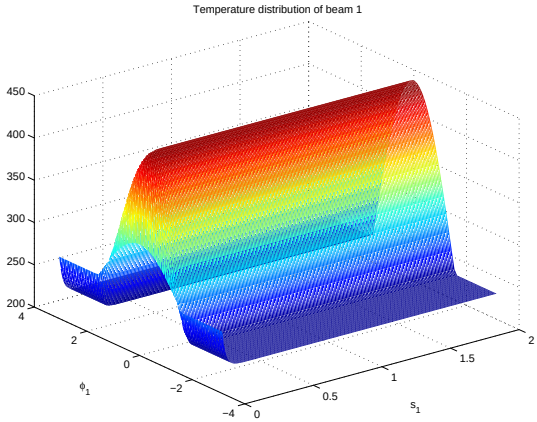

Figure 16: Temperature distribution on beam 1, $\xi_1 = 0$, $\xi_2 = \frac{\pi}{2}$, $T^* = 290\ K^o$, $\lambda_L^1 = 100$, $\lambda_R^1 = \lambda_L^2 = \lambda_R^2 = 0$

average temperature of the beam. The boundary flux parameters where taken to be $\lambda_L^1 = \lambda_R^1 = \lambda_L^2 = \lambda_R^2 = 10^5$. Figure 18 show the transverse deflections and axial displacements while Figure 17 depicts the temperature distribution on beam 1 for this case (the temperature distribution for beam 2 is exactly the same) . Also Figure 19 shows the circumferential temperature gradient $T^{m,1}(s_1)$.

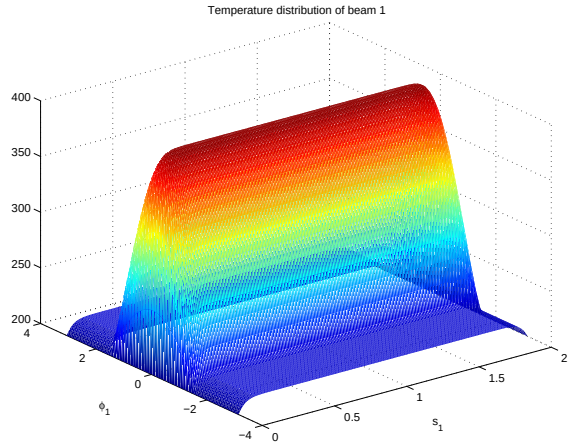

Figure 17: Temperature distribution on beam 1, $\xi_1 = -\frac{\pi}{4}$, $\xi_2 = \frac{\pi}{4}$, $T^* = 200\ K^o$, $\lambda_L^1 = \lambda_R^1 = \lambda_L^2 = \lambda_R^2 = 10^5$

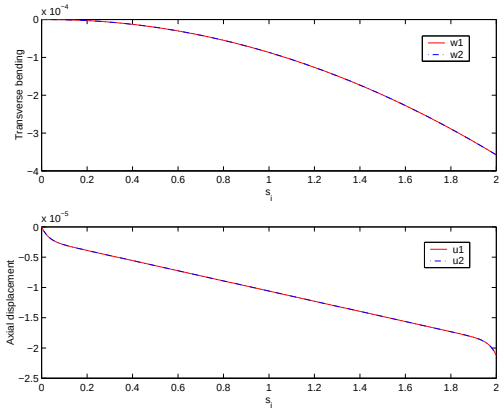

Figure 18: Transverse and axial deflections of beam 1, $\xi_1 = -\frac{\pi}{4}$, $\xi_2 = \frac{\pi}{4}$, $T^* = 200\ K^o$, $\lambda_L^1 = \lambda_R^1 = \lambda_L^2 = \lambda_R^2 = 10^5$

Experiment 8: For this experiment all values where the same as for Experiment 7 except that now the external temperature was chosen to be $T^* = 400\ K^o$, i.e. a value much higher than average temperature of the beam. Figure 21 show the transverse deflections and axial displacements while Figure 20 depicts the temperature distribution on beam 1 for this case. Also Figure 22 shows the circumferential temperature gradient $T^{m,1}(s_1)$.

Finally we include some results obtained for the case in which the material used for the beams is

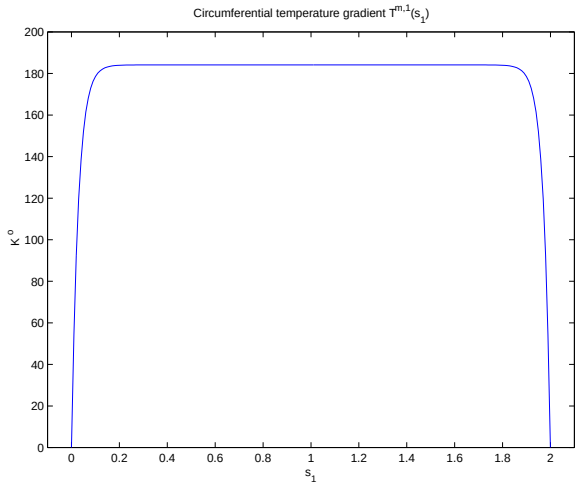

Figure 19: Circumferential temperature gradient, $T^{m,1}(s_1)$, $\xi_1 = -\frac{\pi}{4}$, $\xi_2 = \frac{\pi}{4}$, $T^* = 200\ K^{\text{o}}$, $\lambda_L^1 = \lambda_R^1 = \lambda_L^2 = \lambda_R^2 = 10^5$

aluminum. We took the same parameter values as those appearing in table (1), except for the physical parameters shown in the next table.

Table 2: Physical parameters for aluminum

Parameter	Notation	Value
Material density	$\rho_1 = \rho_2$	$2700\ \mathrm{kg/m^3}$
Young's modulus	$E_1 = E_2$	$75 \times 10^9\ \mathrm{N/m^2}$
Beam's surface (radiation) emissivity	$\epsilon_1 = \epsilon_2$	0.1
Beam's surface (radiation) absorsivity	$\alpha_s^1 = \alpha_s^2$	0.1
Beam's axial thermal conductivity	$k_a^1 = k_a^2$	$20.0\ \mathrm{W/m\,K}$
Beam's circumferential thermal conductivity	$k_c^1 = k_c^2$	$20.0\ \mathrm{W/m\,K}$
Thermal expansion coefficients	$\alpha_1 = \alpha_2$	24.0×10^{-6}

Figure 23 shows the axial and transverse bending for this case under the same conditions of experiment 1. Compare with Figure 3. Note that the transverse bending of beam 1 is about thirty times larger for aluminum than for the composite material while the compression exerted on beam 2 is about 25 times larger in in this case. Similarly, Figure 24 shows the circumferential temperature distribution for this case. Compare with Figure 4. Figure 25 shows the axial and transverse bending for this case under the same conditions of experiment 3. Compare with Figure 7. Once again, the compression exerted on beam 2 is about 25 times larger in in this case.

Figure 26 shows a comparison of the transverse bending in beam 1 for aluminum and composite material under the same conditions of experiment 4. Once again the bending observed at the right boundary is about thirty times larger for aluminum than for composite. Finally, Figure 27 depicts a comparison of the circumferential temperature gradients $T^{m,1}(s_1)$ for aluminum and composite under

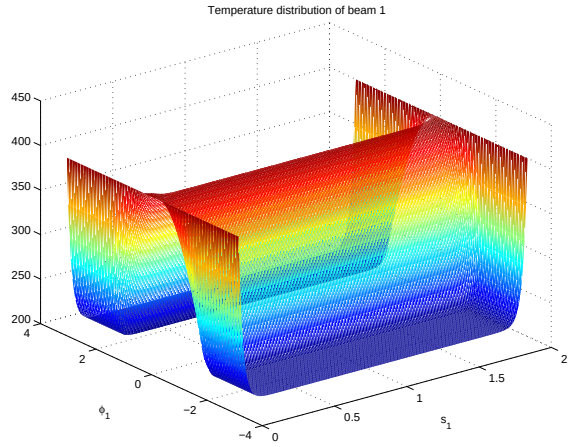

Figure 20: Temperature distribution on beam 1, $\xi_1 = -\frac{\pi}{4}$, $\xi_2 = \frac{\pi}{4}$, $T^* = 400\ K^o$, $\lambda_L^1 = \lambda_R^1 = \lambda_L^2 = \lambda_R^2 = 10^5$

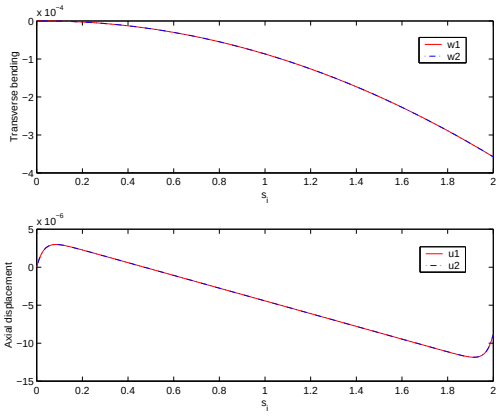

Figure 21: Transverse and axial deflections of beam 1, $\xi_1 = -\frac{\pi}{4}$, $\xi_2 = \frac{\pi}{4}$, $T^* = 400\ K^o$, $\lambda_L^1 = \lambda_R^1 = \lambda_L^2 = \lambda_R^2 = 10^5$

the same conditions of experiment 7.

5 CONCLUSIONS

In this paper we studied the thermo-mechanical behavior of a triangular truss-component consisting of two RI thin-walled circular beams connected through a joint. In the model, transverse and axial mechanical motions of the two beams are coupled though a mechanical joint. The external solar effects were also incorporated by decomposing the temperature fields in the beams. This decomposition lead to two heat equations: one for the circumferential average temperature and one for the axial temperature. The axial temperature is coupled to axial motions of the beam, while the second accounts for a temperature gradient across the beam and is coupled to beam bending. The resulting system of partial and ordinary differential equations formally describes the coupled thermo-mechanical behavior of the joint-beam system. The equilibrium solutions were characterized and several numerical results were presented.

REFERENCES

[1] J.A. Burns, E.M. Cliff, Z. Liu and R. D. Spies, *On Coupled Transversal and Axial Motions of Two Beams with a Joint*, submitted, 2005.

[2] J.A. Burns, Z. Liu and S. Zheng, *On the Energy Decay of a Linear Thermoelastic Bar*. J. of Math. Anal. Appl., Vol. 179, No. 2, 1993, pp 574-591.

[3] E.M. Cliff, B. Fulton, T. Herdman, Z. Liu and R. D. Spies, *Well Posedness and Exponential Stability of a Thermoelastic Joint-Leg-Beam System With Robin Boundary Conditions*, submitted, 2006.

[4] F. L. Huang, *Characteristic Condition for Exponential Stability of Linear Dynamical Systems in Hilbert Spaces*, Ann. of Diff. Eqs., 1(1), 1985, pp 43-56.

[5] C. H. M. Jenkins (ed.), *Gossamer Spacecraft: Membrane and Inflatable Technology for Space Applications*, AIAA Progress in Aeronautics and Astronautics, (191), 2001.

[6] E. A. Thornton and R. S. Foster, *Dynamic Response of Rapidly Heated Space Structures*, AIAA Journal 1992-2207, pp. 1185-1203.

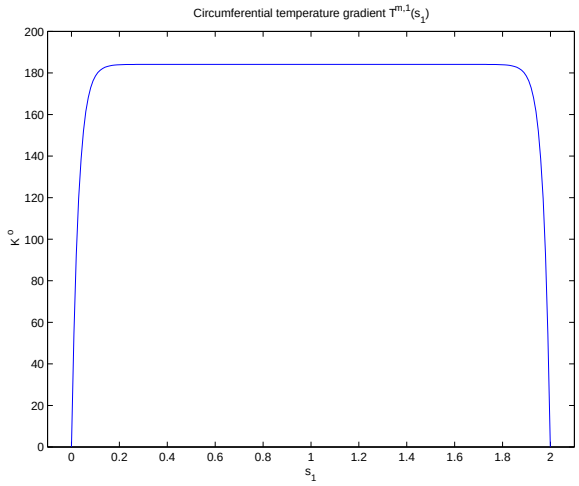

Figure 22: Circumferential temperature gradient, $T^{m,1}(s_1)$, $\xi_1 = -\frac{\pi}{4}$, $\xi_2 = \frac{\pi}{4}$, $T^* = 400\ K^o$, $\lambda_L^1 = \lambda_R^1 = \lambda_L^2 = \lambda_R^2 = 10^5$

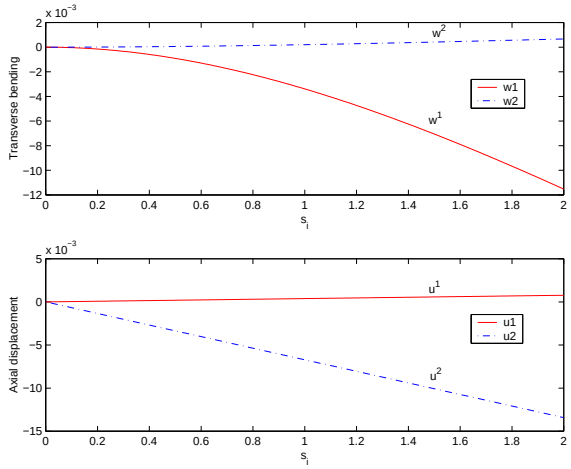

Figure 23: Transverse and axial deflections of beam 1, $\xi_1 = 0$, $\xi_2 = \frac{\pi}{2}$, aluminum.

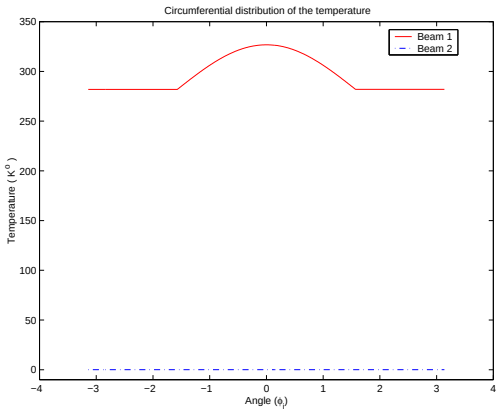

Figure 24: Circumferential temperature distribution, $\xi_1 = 0$, $\xi_2 = \frac{\pi}{2}$, aluminum.

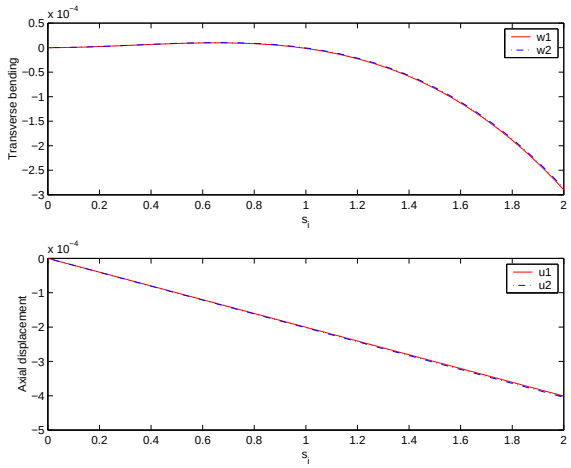

Figure 25: Transverse and axial deflections of beam 1, $\xi_1 = -\frac{\pi}{4}$, $\xi_2 = \frac{\pi}{4}$, aluminum.

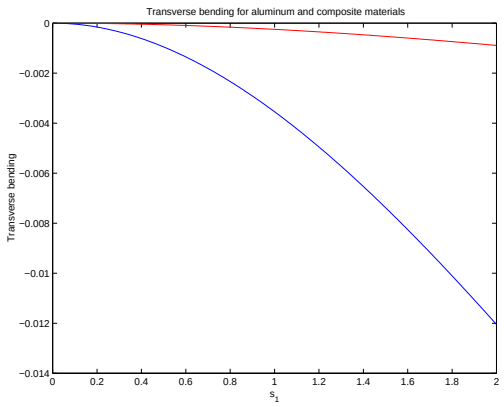

Figure 26: Comparison of transverse deflections of beam 1 for composite and aluminum.

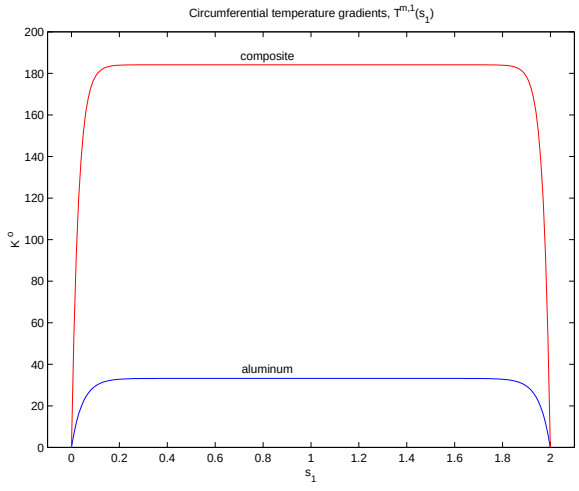

Figure 27: Comparison of the circumferential temperature gradients $T^{m,1}(s_1)$ for composite and aluminum